Vertical directionality and spatial coherence of the sound field in glacial bays in Hornsund Fjord

Hari Vishnu, Grant B. Deane, Mandar Chitre, Oskar Glowacki, Dale Stokes, and Mateusz Moskalik

Citation: The Journal of the Acoustical Society of America **148**, 3849 (2020); doi: 10.1121/10.0002868
View online: https://doi.org/10.1121/10.0002868
View Table of Contents: https://asa.scitation.org/toc/jas/148/6
Published by the Acoustical Society of America

JASA ARTICLE

Vertical directionality and spatial coherence of the sound field in glacial bays in Hornsund Fjord

Hari Vishnu,[1,a),b)] Grant B. Deane,[2,c)] Mandar Chitre,[1,d)] Oskar Glowacki,[3,a),e)] Dale Stokes,[2,f)] and Mateusz Moskalik[3,g)]

[1]*Acoustic Research Laboratory, 12A Kent Ridge Road, National University of Singapore, Singapore 119222, Singapore*

[2]*Scripps Institution of Oceanography, University of California, San Diego, La Jolla, California 92093-0206, USA*

[3]*Institute of Geophysics, Polish Academy of Sciences, Warsaw, Poland*

ABSTRACT:

Arctic glacial bays are among the loudest natural environments in the ocean, owing to heavy submarine melting, calving, freshwater discharge, and ice–wave interactions. Understanding the coherence and vertical directionality of the ambient sound there can provide insights about the mechanisms behind the ice loss in these regions. It can also provide key information for operating technologies such as sonar, communication, and navigation systems. To study the unexplored sound coherence and vertical directionality in glacial bays, a vertical hydrophone array was deployed, and acoustic measurements were made at four glacier termini in Hornsund Fjord, Spitsbergen, in June and July 2019. The measurements show that the sound generated by melting glacier ice is more dominant in the upper portion of the water column near the glacier terminus. The melt water from the submarine melting and the freshwater discharge from the glacier create a glacially modified water duct near the sea surface. This disrupts the inter-sensor vertical coherence in the channel. However, some coherence across the duct is preserved for sound arising from spatially localized events at low frequencies. Overall, the observations in this study can help improve the understanding of the submarine melting phenomenon in glacial bays. © *2020 Acoustical Society of America*.

https://doi.org/10.1121/10.0002868

(Received 29 July 2020; revised 22 October 2020; accepted 11 November 2020; published online 21 December 2020)

[Editor: John A. Colosi] Pages: 3849–3862

I. INTRODUCTION

The Arctic is becoming a hotspot of attention, especially because it is one of the focal points of global climate change (Sutherland *et al.*, 2019). The rise in surface temperature there has been twice as fast as the global average (Overland *et al.*, 2017). A significant component (60%) of the global sea level rise between 2006 and 2015 is attributed to the melting of glaciers and ice-sheets (Oppenheimer *et al.*, 2019). These rapid changes have also spurred an increased technological focus in this region in fields including underwater sonar (Carper, 2017; Hines *et al.*, 2018), communications (Freitag *et al.*, 2016), shipping (Miller and Ruiz, 2014), marine robotics, and oil and gas exploration (Gautier *et al.*, 2009). When operating technologies such as sonar, robotics, and communication devices in the underwater Arctic environment, the spatial coherence and directionality of the acoustic field should be considered. This can help better predict the performance of sonar and communication systems (Freitag *et al.*, 2019; Zhang, 2014), strategize where to optimally place acoustic equipment, or serve as an input to navigational path-planning algorithms to tackle challenges posed by the ambient sound. Knowledge of the spatial correlation structure can also help in strategizing the placement of array sensors so as to maximize the signal-to-noise ratio (SNR) gain (Cron and Sherman, 1962). Recognizing this importance, the directionality and coherence of shallow-water ambient sound have been studied by many authors previously, e.g., Buckingham (1981,1997), Deane *et al.* (1997), Harrison (1996), and Kuperman (1980), in the context of sources such as wind-induced breaking waves and shipping. This work examines the vertical directionality and coherence of ambient acoustic sound in an Arctic glacial bay.

Acoustics is a suitable tool to probe underwater environments over long ranges in the Arctic as sound waves propagate better in water as compared to electromagnetic waves. Characterizing the acoustic field in the Arctic is key to better understanding and exploring this region. It is also crucial for improving the performance of various technologies deployed there. Acoustical studies, starting from the 1960s (Macpherson, 1962; Milne and Ganton, 1964), have explored the seasonality, directionality, and statistics of the noise in the Arctic. Urick (1971) showed that melting glacier ice generates impulsive underwater sound due to the release of air bubbles in the glacier ice. These bubbles have

[a)]Also at Scripps Institution of Oceanography, University of California, San Diego, La Jolla, CA 92093-0206, USA.
[b)]Electronic mail: harivishnu @gmail.com, ORCID: 0000-0002-1617-959X.
[c)]ORCID: 0000-0002-4848-8637.
[d)]ORCID: 0000-0001-6243-7871.
[e)]ORCID: 0000-0002-5164-0206.
[f)]ORCID: 0000-0002-2243-5078.
[g)]ORCID: 0000-0002-0615-9528.

gas pressures approaching 2 MPa (Scholander and Nutt, 1960). Some of them are released explosively from the melting ice, creating impulsive transients that can have peak pressures of over 100 Pa (Deane *et al.*, 2019). A considerable amount of research has been undertaken on the acoustics in the Arctic open ocean, fjords, and sea-ice covered environments and the processes behind it (e.g., Collins *et al.*, 2019; Dziak *et al.*, 2015; Pettit, 2012; Pettit *et al.*, 2012; Pritchard, 1990; Sanjana *et al.*, 2018). Long-term monitoring studies based on acoustics have been proposed in the Arctic open ocean (Kinda *et al.*, 2013, 2015) and at glaciers (Deane *et al.*, 2014; Schulz *et al.*, 2008).

Among Arctic environments, the sound in glacial bays particularly poses a challenge due to its high levels, time-varying nature, and distinct statistical properties (Deane *et al.*, 2014; Głowacki *et al.*, 2015; Pettit *et al.*, 2015). Studies around the world have shown that glacial bays are among the loudest natural environments in the ocean. The sound levels in these regions in calm weather conditions are comparable to those reported in the open ocean at Sea State 4 or higher (Tegowski *et al.*, 2011). The ambient soundscape arises from a rich array of spatially diverse sources radiating sound in distinct spectral bands (Deane *et al.*, 2014; Pettit *et al.*, 2012). The sound field has different statistical properties in different bands as noted by Tegowski *et al.* (2011). Furthermore, the changing thermohaline structure of the water column across seasons significantly alters the sound-speed profile (SSP) and impacts sound propagation in the region (Glowacki *et al.*, 2016).

Apart from providing key input for effective use of underwater technologies, understanding the coherence and vertical directionality in the Arctic can also reveal insights into the physical processes driving the soundscape in this region. In the context of the Arctic, Glowacki *et al.* (2018) studied the directionality of underwater sound from melting icebergs, whereas Zakarauskas and Thorleifson (1991) described the directionality of ice-cracking sounds under sea ice. Poulsen and Schmidt (2016) reported vertical directionality measurements in the Arctic Ocean in the presence of the Beaufort lens, showing that most of the ambient sound comes in at angles close to the horizontal plane. However, studies on the coherence and directionality of the ambient sound in the challenging environment encountered in glacial bays have been limited. To date, the horizontal directionality in glacial bays has been studied (Deane *et al.*, 2014; Głowacki *et al.*, 2015), and the effect of the thermohaline structure of the water channel on acoustic propagation has been reported (Glowacki *et al.*, 2016). Preliminary vertical directionality measurements in Svalbard showed that the majority of the acoustic energy from submarine glacier melting (SGM) emanated from the top tens of meters of the underwater part of the glacier terminus (Deane and Glowacki, 2018). There has been no detailed study on the vertical directionality and spatial coherence of the ambient soundscape in glacial bays so far.

In order to study these aspects of the ambient sound in glacial bays, a vertical hydrophone array was deployed and acoustic measurements were made in Hornsund Fjord, Spitsbergen, in June and July 2019. This paper is organized as follows. Section II discusses details of the experiment undertaken in Spitsbergen to collect data and how this region compares with glacial bays in other regions. Section III discusses the sound sources observed in this region, Sec. IV analyzes their vertical coherence, and Sec. V presents the results on the vertical directionality of the sound. Conclusions are drawn in Sec. VI.

II. EXPERIMENT DETAILS AND STUDY REGION

The study area includes the glacial bays of four glaciers—Hansbreen, Paierlbreen, Muhlbacherbreen, and Samarinbreen [locations in Fig. 1(a) and field deployment photos in Figs. 2(b) and 2(c)]. These are polythermal glaciers having a mixed basal thermal regime, consisting of both warm ice (at close to the melting point at prevalent pressure conditions) and cold ice (below the melting point; Glasser, 2011). The total area of the glacier cover in Hornsund Fjord has diminished by approximately 172 km^2 in the period from 1899 to 2010 (Błaszczyk *et al.*, 2013). With a positive mean annual trend in temperature of 1.14 °C per decade in the last four decades, this region has been warming at a rate that is six times higher than the global average (Wawrzyniak and Osuch, 2020). Tidewater glaciers constitute 97% of the glacierized areas in Hornsund. On an average, they lose 40% of their mass via frontal ablation (Błaszczyk *et al.*, 2019), and their retreat rate is higher than the average of other Svalbard tidewater glaciers. This is likely due to the entry of warm waters of the West Spitsbergen Current and the warm marine climate, which make this region more sensitive to climate change (Błaszczyk *et al.*, 2013). Bathymetric surveys indicate the mean fjord depth in this region is 93 m (Moskalik *et al.*, 2013).

The ambient sound field in these glacial bays, as well as in similar ones in Alaska and Antarctica, is attributed to four main sources—iceberg calving, SGM, freshwater discharge, and ice–wave interactions (Deane *et al.*, 2014; Pettit *et al.*, 2012). Calving is defined as a mechanical loss of ice from glaciers and ice shelves (Benn *et al.*, 2007), and freshwater discharge refers to the discharge of meltwater from the glacier, which results from surface melting. Natural sources like rain and wind-induced breaking waves, biological sources, and anthropogenic sources, such as shipping, also make contributions that are time and location dependent. The ambient sound level exhibits temporal and spatial variations induced by seasonality or variation of the sources and environmental factors such as thermohaline structure of the bay, bathymetry, ocean-surface conditions, and weather.

The sound field in glacial bays in Hornsund may contrast glaciers in other regions which are characterized by the presence of ice-tongues, sea ice, or ice melanges.[1] The sea ice season in Hornsund starts by late autumn or winter (Muckenhuber *et al.*, 2016). On the other hand, glaciers in West or Southeast Greenland are characterized by the presence of sea ice, modulated by oceanic and atmospheric

https://doi.org/10.1121/10.0002868

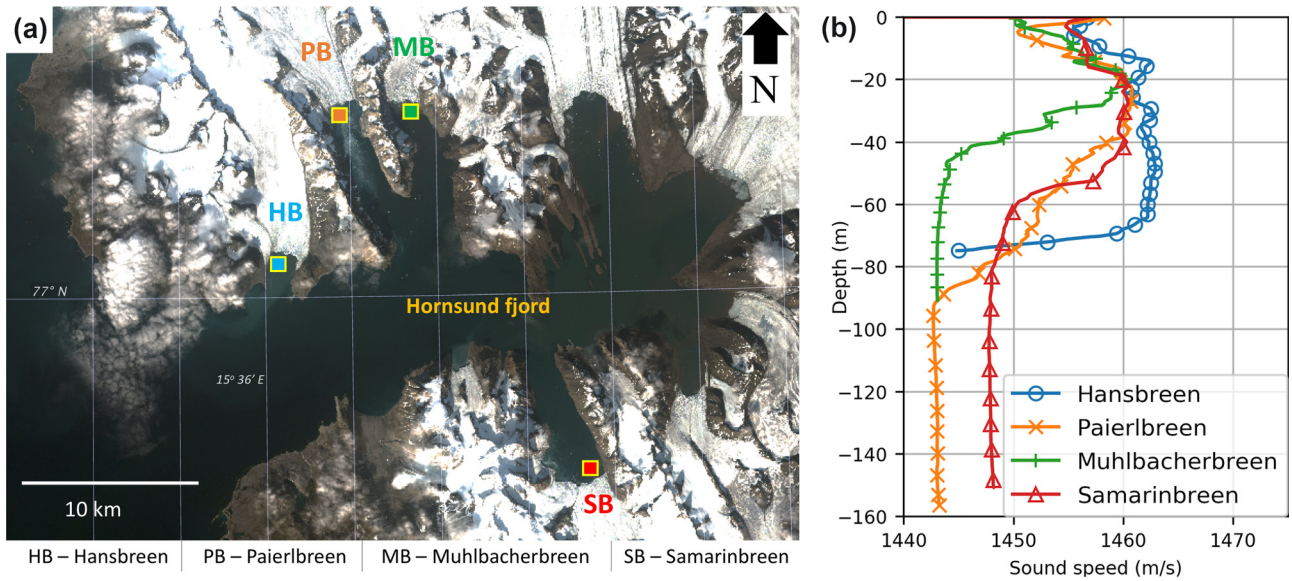

FIG. 1. (Color online) (a) Map of Hornsund Fjord where measurements were taken. Square boxes indicate the areas where acoustic measurements were taken. The satellite image is courtesy of Sentinel-2A [Earth Resources Observation and Science (EROS) Center, 2020] via the United States Geological Survey (USGS) Earth Explorer. (b) SSPs in the four glacial bays measured using conductivity-temperature-depth casts.

forcing (Straneo *et al.*, 2013; Straneo *et al.*, 2012). In the presence of sea ice or ice melanges, additional mechanisms not mentioned above may contribute to the sound field, such as ice fracturing, ridging, surface waves, wind–ice interactions, and thermal cracking (Lewis and Denner, 1988; Sagen *et al.*, 1990), and the sound level has been described as statistically non-Gaussian (Milne and Ganton, 1964). These regions may also see higher contributions to the ambient sound due to ice-ice collisions. Overall, these would lead to the sound field in sea-ice covered bays having different characteristics from the examples discussed in this paper.

To study the thermohaline properties, conductivity-temperature-depth casts were used to make estimates of the SSP in the four bays, shown in Fig. 1(b). While there is a large spatial variability observed from one bay to another, one common feature in all of them is the presence of a near-surface low-soundspeed layer due to the intrusion of freshwater from the SGM and subglacial discharge at the glacier.

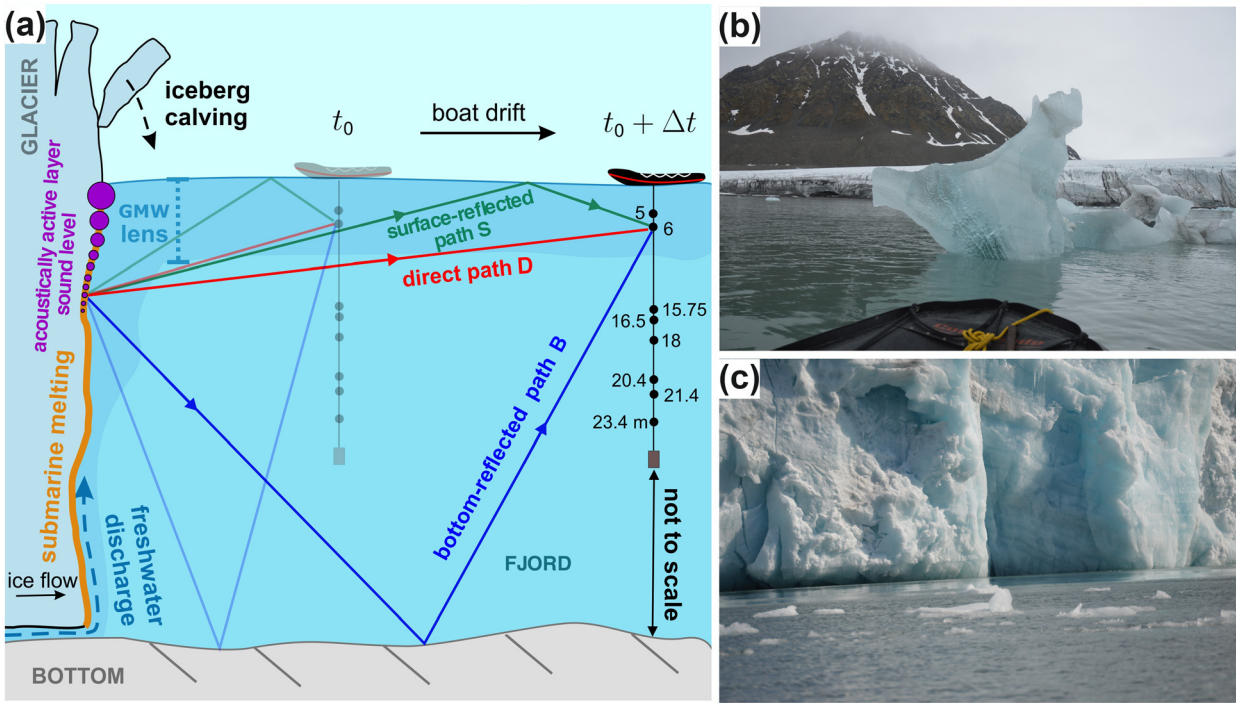

FIG. 2. (Color online) (a) Illustration of the field setup for the directionality measurement and (b),(c) photos from field deployments.

This glacially modified water (GMW) occupies a surface layer reaching down to about 15–20 m below the surface. Due to this, the sound velocity changes with a positive gradient of about 0.55 m/s/m from just below the surface down to about 20 m (averaged for the four bays). Owing to the presence of this GMW duct, a highly upward-refracting profile is created inside the subsurface layer (Glowacki *et al.*, 2016). Such GMW layers have been observed spanning over large horizontal areas in other regions as well, such as Alaska, Greenland, and Antarctica (Arimitsu *et al.*, 2016; Jacobs *et al.*, 2011; Jenkins and Jacobs, 2008; Straneo *et al.*, 2011). It will be seen later in this paper that this GMW duct plays an important role in shaping the coherence of the acoustic field in the glacial bays.

This thermohaline structure is observable for glacial bays in Svalbard between the end of May and November (Glowacki *et al.*, 2016). However, it does not hold true throughout the year because the ocean temperatures can show large variations. Neither is this picture fully representative of the environments found in other glacial bays. In Alaska, such thermohaline processes also occur in winter, whereas in Antarctica, the ocean water temperature is strongly influenced by weather patterns, sea ice conditions, and the effect of the Antarctic Circumpolar Current (Deane *et al.*, 2019; Moffat and Meredith, 2018). While the GMW duct span is observed to be 10–20 m in Hornsund, glaciers in other locations may have deeper GMW layers, such as up to 200 m depth in parts of Greenland (Straneo *et al.*, 2011) or Antarctica (Cape *et al.*, 2019; Jacobs *et al.*, 2011; Jenkins and Jacobs, 2008).

To summarize, while the study in this paper gives insight into the sound field in glacial bays in Hornsund Fjord during the summer to fall months, it is not necessarily fully representative of the acoustics at other times or in other glacial bays.

To study the sound field in the region, underwater sounds were recorded from a boat using an eight-element 18.4 m-long vertical hydrophone array [illustrated in Fig. 2(a)]. The array elements will henceforth be referred to by their order on the array, beginning from the topmost hydrophone. The hydrophones were mounted on a line and non-uniformly separated. Audio was captured at a sampling rate of 96 kHz. To keep the array vertical, a weight was attached to the end of the array line. However, the array still exhibited a small amount of tilt due to the drag from the flow of water. In order to detect the tilt, depth sensors were mounted on the array line at two positions—0.34 m below the surface mark and 0.34 m below hydrophone 8. Measures were taken to reduce the effect of flow-induced strum noise on the array recordings at high frequencies. Despite this, some contamination from strum noise was observed at low frequencies (below ∼100 Hz). The bottom depth was logged using a Lawrence echosounder, and photographs supplemented with compass data were taken from the boat. During the trials, detailed logs were made of other events occurring in the bay, such as calving and passing chunks of ice, that were close enough to contribute significantly to the acoustic recordings. Additionally, the Global Positioning System (GPS) location of the boat was logged, and the range to the closest point of the glacier face was measured using a laser-based distance measurement device. Ranges were also measured to floating ice pieces that came close to the array. The pieces of ice that have broken off from the glacier are referred to as growlers if they have less than 1 m showing above water (National Snow and Ice Data Center) and as bergy-bits if they have more than 1 m but less than 5 m showing above the water (National Snow and Ice Data Center).

In this work, the focus is on three dominant natural sources in the Hornsund Fjord region, namely SGM, calving, and melting of drifting ice pieces. Each one of these has distinct spectral signatures and spatial coherence properties. Characteristics of other natural sources (e.g., wind-induced breaking waves, rain) and anthropogenic sources (e.g., shipping) have been well-studied in the literature and, hence, will not be considered here.

The most dominant and steadily observed sound is that of SGM. It is strongest in the 0.5–3 kHz band but contains energy all the way up to 15 kHz and beyond [Figs. 3(a) and 3(c)]. It arises due to a superposition of numerous bubble explosion events occurring across the face of the glacier. SGM produces a steady signal with near-Gaussian statistics, consistent with observations by Tegowski *et al.* (2011, 2012) and Glowacki *et al.* (2018) on the sound at frequencies above 2.5 kHz. This is because at sufficiently large distances from the glacier, the acoustic time series observed at the hydrophones arises from numerous bubble explosion events originating from a large area of the glacier terminus. Thus, the time series is not characterized by a few strong and dominating outlier events originating from a small region of the glacier face. Rather, it has an envelope of nearly constant magnitude, which gives rise to a Gaussian distribution. Figure 3(a) is a plot of the spectrogram of a 10-s recording when the closest point at the glacier wall was 273 m away from the array. The recording contains SGM background sounds and a calving event at 5 s. The power spectral density (PSD) of SGM is compared against other sounds in Fig. 3(c).

Occasionally, calving events occur in the bay where icebergs detach from the glacier terminus and impact the sea surface. This produces intermittent impulsive transient sounds through the various phases of the calving event (Glowacki, 2020; Pettit, 2012). Each of these phases emits sound signatures in different bands [see Figs. 3(a) and 3(c)], spanning from very low frequencies (∼20 Hz) up to 30 kHz. Previously, Tegowski *et al.* (2011, 2012) have observed that the ambient sound in the spectral band corresponding to calving is statistically non-Gaussian, predominantly due to the effect of these impulsive transients. For calving events in Hornsund Fjord bays, the source levels can go over 200 dB re 1 μPa at 1 m from the point of impact (Glowacki and Deane, 2020). The levels recorded at the hydrophones depend largely on the depth and distance of the hydrophone from the point of impact.

https://doi.org/10.1121/10.0002868

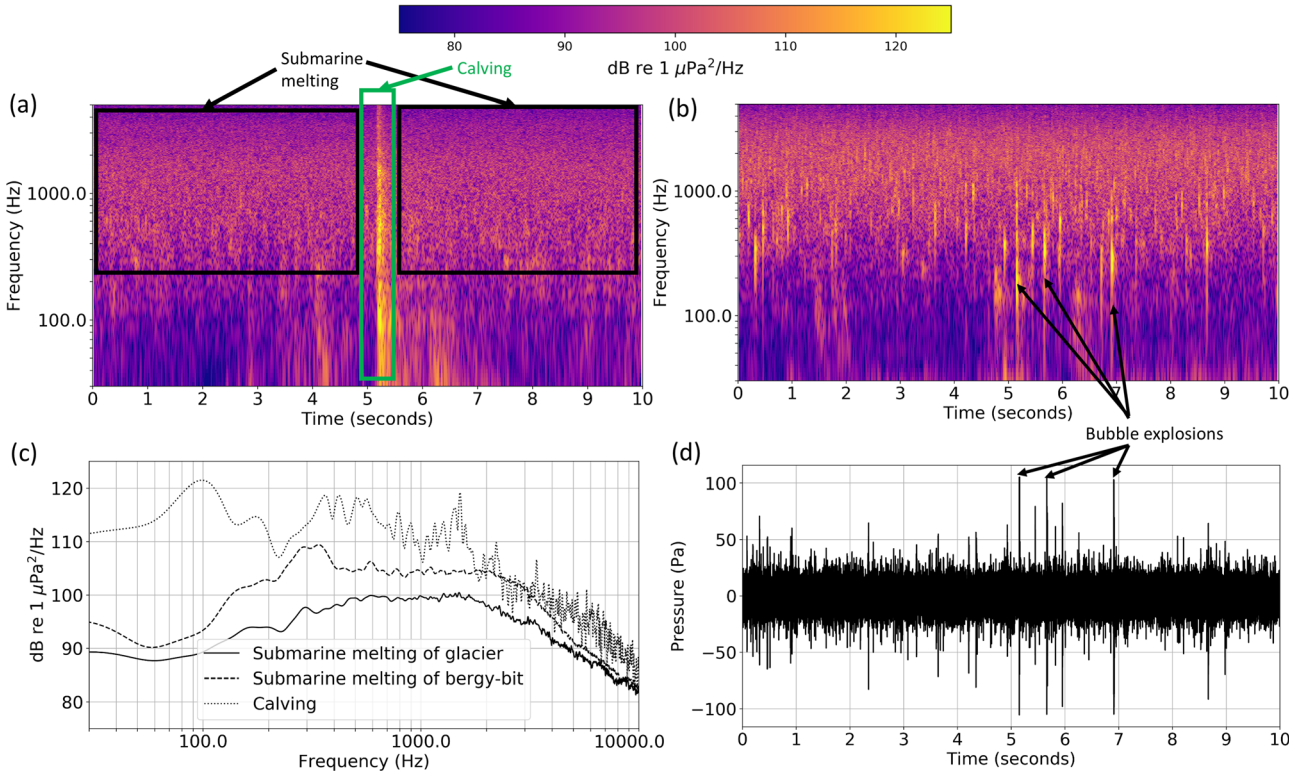

FIG. 3. (Color online) (a) Spectrogram of a 10-s sound clip containing SGM and calving sounds, (b) spectrogram of 10-s clip where a bergy-bit was close to the hydrophone, (c) the power spectral density (PSD) of different events, and (d) time series of a 10-s clip where a bergy-bit was very close to the hydrophone.

III. SOUND SOURCES

The ice pieces resulting from calving float around in the bay and undergo melting due to contact with seawater. The observed acoustic signature of melting ice pieces is largely dependent on their distance from the recording instrument. The statistics of the sound produced by nearby ice pieces is non-Gaussian. This is because the heterogeneity of individual bubble explosions observed at a nearby receiver leads to a heavy-tailed distribution (Glowacki *et al.*, 2018). Figure 3(b) shows the spectrogram of a 10-s recording at a hydrophone when a bergy-bit was close to the array (7 m away). The spectrum of the bergy-bit melting is similar to that of SGM [Fig. 3(c)]. However, in the example shown, the former is recorded at a higher sound level (4 dB higher at 1 kHz) due to the proximity of the bergy-bit. Qualitatively, the impulsive events indicating the bubble explosions are more clearly visible in the spectrogram and time series of the bergy-bit's melting sound [Figs. 3(b) and 3(d), respectively] as compared to the spectrogram of SGM [Fig. 3(a)].

IV. VERTICAL COHERENCE

In Figs. 4–6, inter-hydrophone coherence curves are plotted for different types of acoustics events. The coherence $\Gamma(f)$ at a frequency f between any two hydrophones i and j is defined as (Cox, 1973)

$$\Gamma(f) = \frac{\langle S_i(f) S_j^*(f) \rangle}{\sqrt{\langle S_i(f) S_i^*(f) \rangle \langle S_j(f) S_j^*(f) \rangle}}, \quad (1)$$

where $S_i(f)$ is the Fourier transform of the pressure time series at hydrophone i. The symbols "*" and $\langle\,\rangle$ denote complex conjugation and the ensemble average, respectively. The coherence is computed from a clip of recorded data as

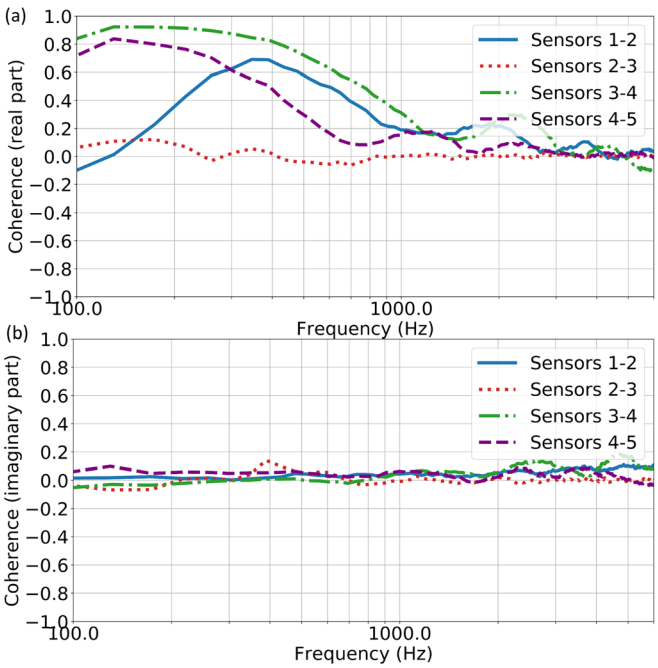

FIG. 4. (Color online) (a) Real part and (b) imaginary part of spatial coherence among neighboring sensors in the top five hydrophones, computed over a 4-min-long recording of SGM sound at Paierlbreen.

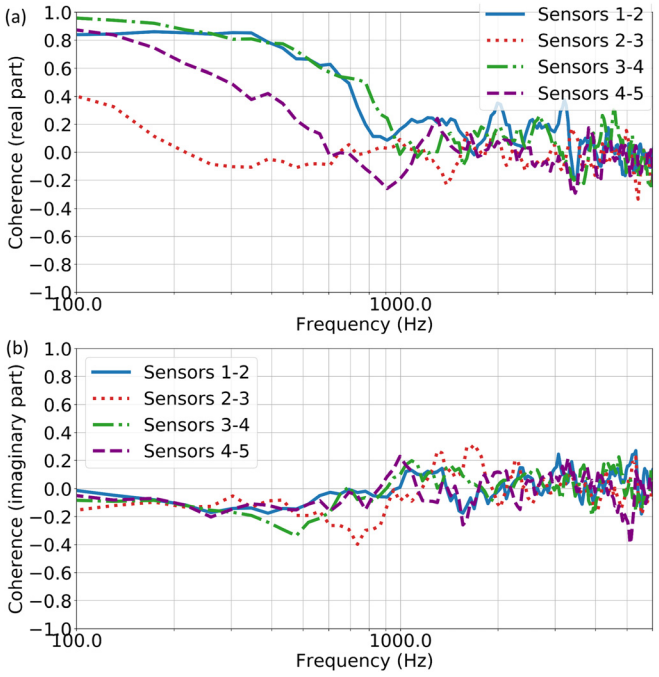

FIG. 5. (Color online) (a) Real part and (b) imaginary part of spatial coherence among neighboring sensors in the top five hydrophones, computed over a 0.7-s-long recording at Hansbreen glacier when a calving event occurred.

follows. The clip duration is split into segments of 23 ms each. The overlap between successive segments is 50% for the cases of Figs. 4 and 6 and 99% for Fig. 5 (because the clip is of much smaller duration in this case). The terms $S_i(f)S_j^*(f)$, $S_i(f)S_i^*(f)$, and $S_j(f)S_j^*(f)$ are computed for each segment for all sensor-pairs considered. Then, the average value of these terms over all the segments is computed and used to estimate the coherence as in Eq. (1). At frequencies of around 100 Hz and below, noise from sources such as strum and water-flow turbulence begins to dominate the sound level and coherence in the recordings. Hence, we plot the coherence curves only for frequencies greater than 100 Hz.

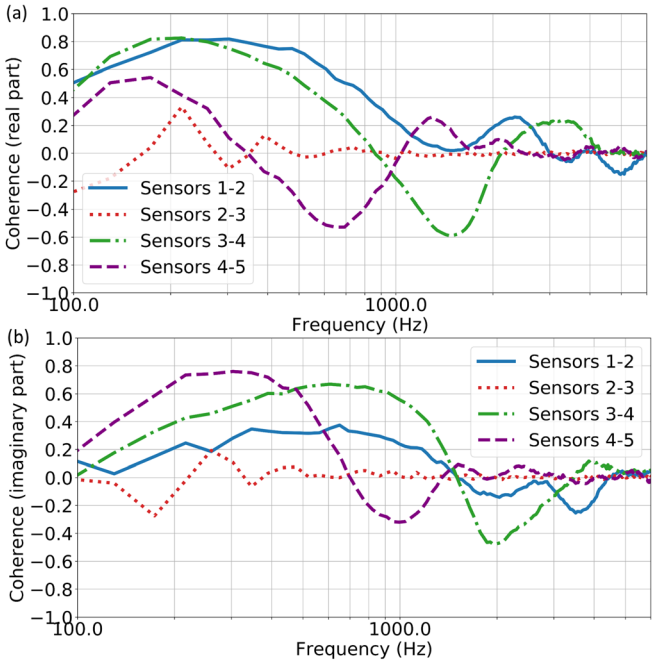

FIG. 6. (Color online) (a) Real part and (b) imaginary part of spatial coherence among neighboring sensors in the top five hydrophones, computed over a 4-min-long recording at Hansbreen glacier when a bergy-bit was nearby.

Figure 4 shows the vertical coherence of the ambient sound due to SGM during a 4-min recording at Paierlbreen. During this period, only the SGM sound contributed to the coherence as no other acoustic events were noted. The coherence is plotted between neighboring hydrophone pairs for the top five hydrophones. The coherence between the remaining three neighboring sensor pairs (5–6, 6–7, 7–8) show similar trends as 3–4 and 4–5.

In Fig. 4, the vertical coherence magnitude between sensors 2 and 3 is lower than other sensor pairs, which is explained as follows. Sensors 1, 2, and 3 were at depths of 5 m, 6 m, and 15.8 m, respectively [refer Fig. 2(a)]. As seen in Fig. 1(b), the near-surface zone of the water channel had a layer of cold GMW until a depth of 15 m, which led to an acoustic duct being formed in this zone. The top two sensors were located within this duct. Thus, they recorded SGM sound trapped within the duct and carried over longer ranges. However, this was not the case with the bottom six sensors, which were located below the duct. Therefore, when recording SGM sound, these two subgroups are coherent within themselves but incoherent with each other. The coherence of the top two sensors indicates that the duct may be fairly stable over a large horizontal area of the bay spanning from the glacier face to the array.

Figure 5 shows the vertical coherence of a short sound clip recorded at Hansbreen when a calving event occurred. Here, the coherence curves are smoothed by applying a moving-average filter of width 66 Hz to smooth the oscillations which arise because the clip is short. As in Fig. 4, the coherence between sensors 2 and 3 is lower than between other sensor pairs. It begins to increase at low frequencies ($<$200 Hz). There are two possible reasons for this. First, the noise from the calving is impulsive and excites a large band of low frequencies spanning until about 3 kHz. At low enough frequencies, the sound wavelength is comparable to the vertical span of the GMW duct. Hence, geometric ray acoustics is not necessarily accurate in this regime, and the duct does not trap sound and disrupt coherence at low frequencies as much as it does at higher frequencies. The frequency below which the coherence between sensors 2 and 3 increases (150 Hz) corresponds to a wavelength of 10 m, which is on the order of the vertical span of the duct. This lends some validation to the above explanation for the observed coherence. The second possible reason is that the calving event is a more spatially localized source as compared to SGM. The sound waves arriving at all the sensors from this localized source are more coherent because they pass through a very similar cross section of the channel and arrive at the sensors with varying phases. On the other hand,

https://doi.org/10.1121/10.0002868

for a distributed source like SGM, the inter-sensor phase relationship varies for waves arriving from different originating locations of the source. This leads to reduced overall coherence between the sensors when the combined effect of the distributed source (SGM) is taken into account.

Figure 6 shows the vertical coherence of the ambient sound recorded at Hansbreen when a bergy-bit was passing by close to the array. The notable difference here as compared to Fig. 4 is that the imaginary component has a larger magnitude. This is because of the greater asymmetry in the vertical sound field due to the proximity of the bergy-bit (Deane *et al.*, 1997). In the case of Fig. 6, the recorded data consist mostly of downward traveling sound arising from the bergy-bit. However, in the case of sound from SGM, the field is not strongly asymmetric about the horizontal because the sound from the glacier terminus arrives at the sensors with less steeper angles of arrival (AOAs).

V. DIRECTIONALITY RESULTS

The vertical directionality of recordings from each of the four glacial bays is analyzed in this section, using the bottom six sensors of the array. This decision is based on our coherence estimate of the SGM sound (Fig. 4), which showed that the top two sensors are uncorrelated with the rest of the array. The acoustic waves received at the array are assumed to have a planar wavefront. This assumption works reasonably well in practice for the frequencies considered in our processing because the array is far enough from the glacier wall. A normalized coherent array-processing approach is used to estimate the directionality, inspired by the matched-field source localization algorithm developed by Michalopoulou and Porter (1996). In this broadband method, the linearly beamformed pressures are summed across all the frequency bands considered in the processing after normalizing the phase and amplitude. This method allows us to negate the effect of sidelobes in the array response and obtain better resolution by coherently combining information across frequency bands rather than incoherently averaging across frequencies. As seen in Fig. 3, the acoustic power of SGM is highest in the 1–3 kHz band, and it tapers off at higher frequencies. However, there is still sufficient information and SNR at frequencies up to 15 kHz. Hence, a frequency range of 0.5–15 kHz is used to estimate the directionality.

A. Propagation modeling

In addition to plotting the directionality estimates, we explain the observed patterns using the ray-tracing propagation model Bellhop (Porter, 2011; Porter and Bucker, 1987). This modeling is based on our knowledge of the experimental setup and provides additional insight into the observed results. Bellhop can model the effect of the range-varying bathymetry and the near-surface sound duct on the acoustic raypaths for wavelengths smaller than the span of the duct. The sediment bottom is assumed to be a half-space with sound speed, density, and attenuation of 1530 m/s, 1.4 g/cm^3, and 0.1 dB/m/kHz, respectively. These are typical values for clayey silt (Hamilton, 1976), which is a common type of sediment in Hornsund (Staszek and Moskalik, 2015).

There are some uncertainties in the experimental setup that influence our modeling:

(1) While our depth sensors indicated the direction and trend of the array tilt, they were too noisy to yield a useful estimate of the tilt. Thus, the tilt is estimated from the observed directionality using the depth-sensor information as a guideline.
(2) The SSP is expected to exhibit spatio-temporal variations across the bay. This is especially true at the glacier-ocean boundary due to processes such as freshwater discharge and calving. However, the SSP variation over the entire channel is not known to us. Therefore, the channel's SSP is assumed to be time and range invariant within each glacial bay and equal to that measured by us at one location in the bay [Fig. 1(b)].
(3) The bathymetry of this region is not completely known, especially near the glacier front. It is risky to make depth measurements close to the calving glacier fronts, and accurate measurement is difficult due to the high retreat rate of tidewater glaciers. The lack of bathymetry at tidewater glaciers is a challenge in other polar regions as well, e.g., in Greenland. A part of the bathymetry for the region under study is estimated by interpolating the point depth measurements made from the boat. For regions outside the boat transects, no information is directly available to discern the bathymetry. Therefore, to fill in the gaps in bathymetry for such regions, we use the information from the directionality plots to obtain feasible values of bathymetry that can explain the trends in the plots, which are also consistent with the available depth measurements.

Due to the uncertainty in bathymetry and SSP, the model predictions may show some deviations from the data. Despite this, it is instructive to compare our estimates against a model because it allows us to understand the data better, accounting for propagation effects as much as possible.

Finally, note that the SGM sound arises as a result of melting across the entire submerged face of the glacier. However, incorporating the full horizontal extent of the glacier in modeling is not straightforward. For the sake of simplicity, it is assumed that the observed directionality is influenced most by the sources nearest to the vertical array—these correspond to the region of the glacier-ocean interface closest to the array. Regions of the interface that are further away from the array would contribute weaker rays with less steeper AOAs because their horizontal separation with the receivers is larger [see Fig. 2(a)]. Thus, the impact of this assumption in our directionality plots is that each ray arrival exhibits a smear in energy toward less steeper AOAs than modeled. While this assumption is a simplification, it will be seen in the forthcoming results that it works fairly well in explaining the directionality patterns, albeit with some loss of sharpness.

In the forthcoming discussion, it will be shown that the submerged part of the glacier–ocean interface is acoustically active only down to a certain vertical depth as illustrated in Fig. 2(a). We refer to this near-surface region of the interface as the acoustically active boundary layer. Although this is discussed further in the upcoming analyses, we introduce this now for the purpose of setting up the modeling and interpreting its predictions. Inspired by this, the sound field due to SGM is modeled as originating from a number of closely spaced point sources at the glacier-ocean boundary layer. The point sources span a line from the water surface to a depth of 10 m. A two-dimensional (2D) Bellhop model is used to trace raypaths from these sources to the hydrophones of the receiver array. The directionality plots shown in this section are overlaid with Bellhop-predicted AOAs of several raypaths from the source. A letter sequence representing the type of raypath is indicated above each line. *D* stands for the direct path from the source to the hydrophones, *S* stands for the surface-reflected, *B* stands for the bottom-refracted, *BS* stands for the bottom-surface-reflected, and so on.

B. Muhlbacherbreen

In Fig. 7, the directionality observed across the duration of the trial in the bay of Muhlbacherbreen is plotted. The most striking aspect of the sound directionality in Fig. 7(a) is the large band of energy concentrated within the elevation angles −5°–15°. Within this large band, two sub-bands are visible, especially at the start of the trial. The upper and lower sub-bands indicate, respectively, the surface-reflected and direct raypaths from the glacier face to the receiver array.

The concentration of the energy in an angular band around 0° is evidence of the fact that the acoustic energy generated due to melting at the glacier–ocean interface is highest in the uppermost layers of the water, i.e., near the

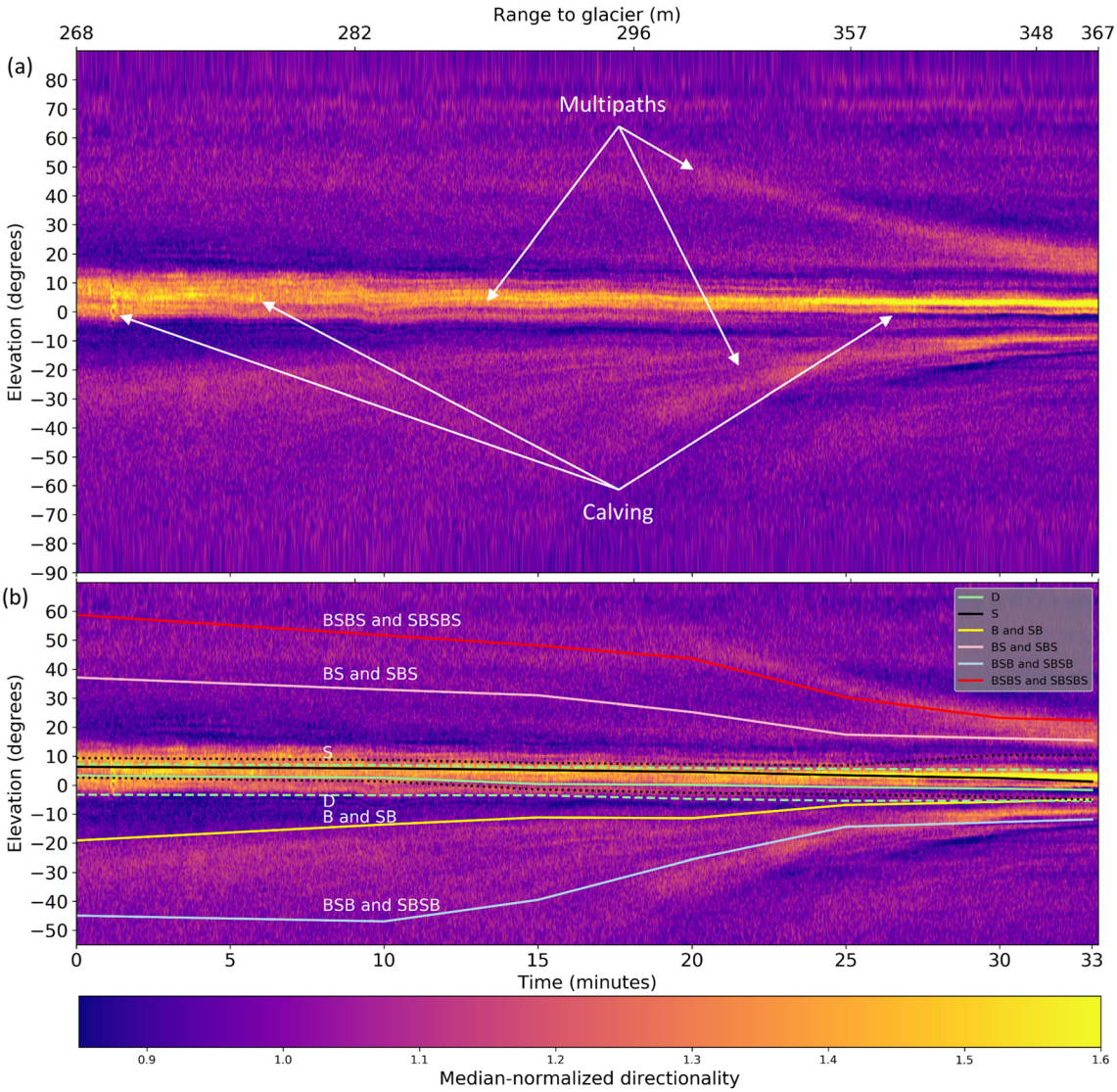

FIG. 7. (Color online) (a) Median-normalized directionality estimate at Muhlbacherbreen and (b) with overlaid model-predicted AOAs. The *x* axis at the bottom shows the trial time, and the *x* axis at the top shows the range to the closest point on the glacier terminus. Solid lines indicate the modeled mean AOA of rays/ray-pairs, and dotted or dashed lines indicate the maximum/minimum AOA of rays.

https://doi.org/10.1121/10.0002868

water surface. Previous experimental studies have also indicated that the sound generated by bubble-release decreases with increasing depth below the surface (Deane and Glowacki, 2018). A likely reason for this lies in the physics of rapid bubble-release from ice. For a bubble newly released from the ice, the energy available to generate sound scales with the difference between the bubble's internal gas pressure and hydrostatic pressure, apart from other factors. If the hydrostatic pressure increases faster with depth than the internal gas pressure within the ice, it would explain the observed decrease in acoustic energy of bubble-releases with depth and, thus, the directionality observed in Fig. 7(a).

The acoustic energy from the *D* and *S* rays is seen to be spread over an angular band. One reason for this is that, as mentioned earlier, the SGM sound arises from a large horizontal span of the glacier face, which is not considered in our modeling. Second, the acoustic source is not a point source. Rather, it is spread over a certain depth, beginning from the water surface, and there could also be contributions from ice debris concentrated along some parts of the glacier terminus. Third, for simplicity of interpretation, our directionality estimation approach assumes that the acoustic waves arriving at the receiver array have a planar wavefront. This assumes that the AOAs of waves at all the hydrophones are equal, which is not necessarily true in reality, contributing to the observed spread.

In order to understand the directionality plot and the angular energy spread in terms of our propagation model, the AOA predictions are overlaid onto the plot in Fig. 7(b). Since the sound field is modeled as arising from sources distributed at the near-surface acoustically active boundary layer, the AOAs of the *B* and *SB* paths are very close to each other and, hence, they are shown together as a pair. Likewise, the AOA of each ray arrival that starts with a

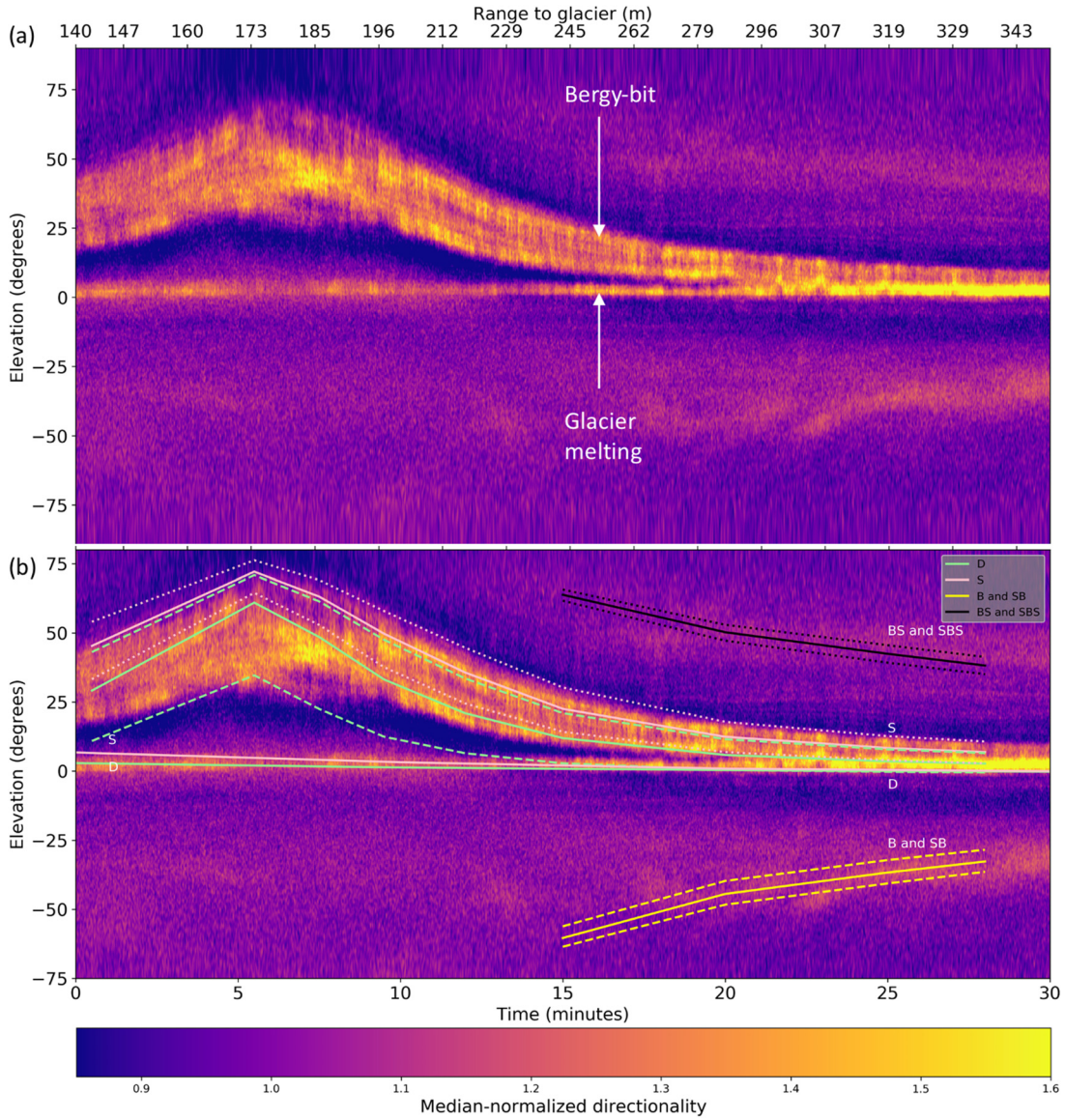

FIG. 8. (Color online) (a) The median-normalized directionality estimate at Hansbreen when a bergy-bit crossed near the boat and (b) with overlaid model-predicted AOAs. The *x* axis at the bottom shows the trial time, and the *x* axis at the top shows the range to the closest point on the glacier terminus. Solid lines indicate the modeled mean AOA of rays/ray-pairs, and dotted or dashed lines indicate the maximum/minimum AOA of rays.

bottom reflection is paired with the corresponding arrival that has a preceding surface reflection. The solid lines depict the modeled mean AOAs of the rays (or ray-pairs) incident at the sensors of the array, whereas the maximum and minimum AOAs corresponding to each path are depicted by the dotted or dashed lines. Together, these define the expected angular band of variation of acoustic energy due to the effects mentioned previously. This convention will be used in directionality plots henceforth.[2]

When the spread in the arrival angle caused due to the effects mentioned above is taken into account in the modeling, the model-predicted AOAs are able to better explain the *D* and *S* path energies in the plots. As the array was moving away from the glacier through the course of the trial, the vertical extent of the energy band shrinks as the trial time progresses. Apart from SGM, acoustic signatures due to subaerial calving events can also be observed in the plot at 1, 6, and 27 min of trial time. These are seen as blips in the −5°–10° band.

C. Hansbreen

During recordings conducted at Hansbreen, a bergy-bit floated very close to the recording array. As per our logs, the bergy-bit was 23 m away from the array at the start of the recording. It reached as close as 5 m at 5.5 min, and then retreated to 147 m by the end of the recording. The bergy-bit's acoustic signature is clearly evident in the directionality plot [in Fig. 8(a)] as a large band of energy that reaches maximum elevation 5.5 min into the trial.

Based on our logs of ranges to the bergy-bit, the AOA of rays from the bergy-bit are modeled. The rays due to SGM are also modeled (*D* and *S* rays only, seen at elevation angles near 0°). These are shown in Fig. 8(b). The vertical spread of energy from the bergy-bit in the directionality plot can be explained to a reasonable degree by assuming that the acoustic energy is contributed by point sources distributed from the water surface down to a depth of 10 m. The *B* ray becomes strongly observable in the plot starting from around 20 min into the trial with an AOA of −50°. The model-estimated angle of incidence of this ray with the bottom is 22° at 20 min. This is consistent with the critical grazing angle of the sediment (19.2°).

D. Samarinbreen

During our trials at Samarinbreen, two growlers passed close enough to the array that their signature was observable in the recordings. In the directionality plots for Samarinbreen (Fig. 9), the contributions from the *S* and *D* rays from these two sources are evident as the arrivals at steeper positive angles.[2,3] The AOAs for rays from the glacier are also indicated—these are the arrivals at near-horizontal angles. The signature due to the first growler is evident from 0 to 27 min as it approaches the array and passes by it at 10 min and then retreats away. From the 27th minute onward, the AOA track of the second growler is observable.

E. Paierlbreen

In Fig. 10, the directionality of the data recorded at Paierlbreen is plotted with model predictions overlaid.[2,3] During the trial, the boat was drifting mostly parallel to the face of the glacier. Thus, the distance from the array to the closest face of the glacier did not vary much over the course of the trial. This explains the relatively unchanging directionality patterns seen in the plot as the trial progresses.

At 10 min into the trial, an underwater calving event occurred at a point on the glacier face that was close to the array. The acoustic signature of this event can be seen in the directionality plot as a streak moving from 6° to 0°. This

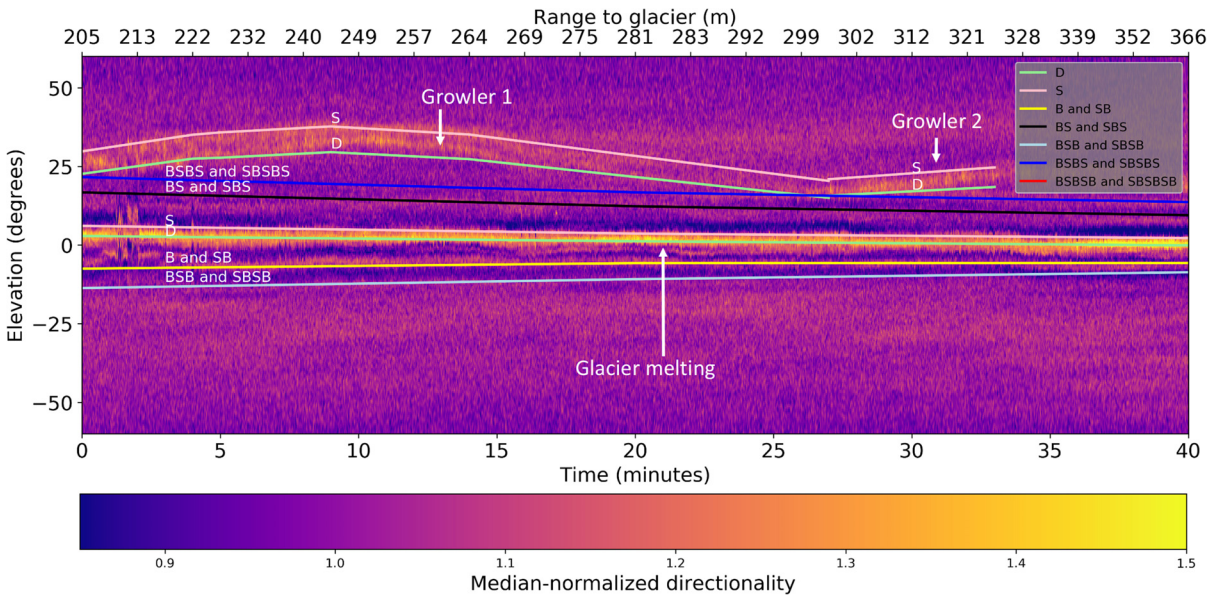

FIG. 9. (Color online) Median-normalized directionality estimate with overlaid model-predicted mean AOAs at Samarinbreen. The *x* axis at the bottom shows the trial time, and the *x* axis at the top shows the range to the closest point on the glacier terminus. Solid lines indicate the modeled mean AOA of rays/ray-pairs, and dotted or dashed lines indicate the maximum/minimum AOAs of rays (footnote 2 and 3).

https://doi.org/10.1121/10.0002868

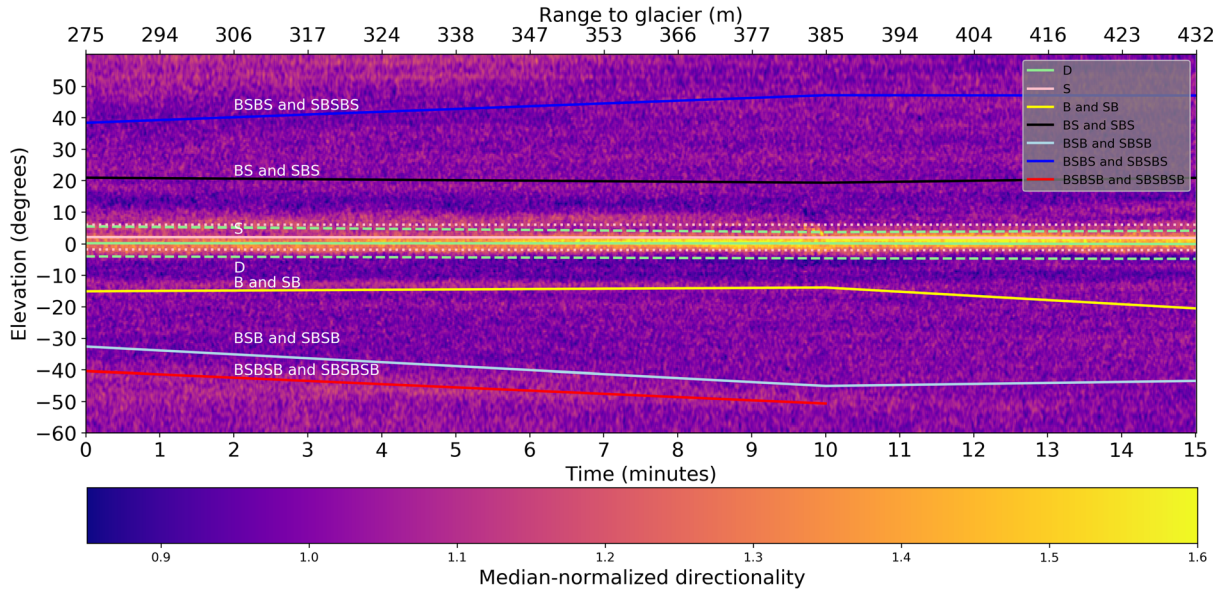

FIG. 10. (Color online) Median-normalized directionality estimate at Paierlbreen with overlaid model-predicted AOAs. The x axis at the bottom shows the trial time, and the x axis at the top shows the range to the closest point on the glacier terminus. Solid lines indicate the modeled mean AOA of rays/ray-pairs, and dotted or dashed lines indicate the maximum/minimum AOA of rays (footnote 2 and 3).

captures the AOA variation of the S ray from the calved ice block as it moved upward toward the water surface. Based on the acoustic track, the calving is estimated to have occurred at a depth of at least 30 m. Another noteworthy observation is that the strength of the S ray from SGM is significantly reduced after the calving event occurs. This is because the surfacing of the calved ice created ripples on the water surface. Due to the rough sea surface no longer playing the role of a strong reflector, the strength of subsequent surface-reflected ray arrivals is weakened.

Most of the energy in the plot falls within −50°–60°. Based on the propagation model and estimated bathymetry, the mean angle of incidence of the $BSBSB + SBSBSB$ ray-pair with the bottom at 0 min is 20°, which is close to the critical grazing angle for the sediment bottom (19.2°). The model-estimated angle of incidence of this ray-pair increases to 50° by 10 min, which explains why the energy from steeper AOAs in the directionality plot reduces as trial time progresses from 0 to 10 min. This is because the increasing incident angle leads to fewer subcritical bounces of the higher-order rays and, thus, less energy of these ray-paths is retained in the channel while more energy is lost into the bottom.

A common feature in all the directionality plots discussed in this section is the band of incoming energy centered near the horizontal direction (within −5°–15°), which is associated with D and S rays from SGM. This is expected to be a stable acoustic feature during months in which SGM takes place. In some scenarios, additional energy is received via B and higher-order multipaths, which account for only a smaller fraction of the energy (for example, ≈35% at 338 m range from Paierlbreen). The directionality plots also exhibit time-varying patterns when calving events occur or when ice pieces pass close to the array. In the case of growlers and bergy-bits, most of the energy is received in the form of D and S paths. These have positive elevation angles larger than those observed for SGM, and the AOA varies as a function of the range to the ice piece.

VI. CONCLUSIONS

This study reports the vertical directionality and coherence of the sound field at four glacial bays in Spitsbergen in summer. To the authors' knowledge, this is the first study to present a detailed analysis of these aspects at glacial fjords. The use of a vertical array yields insights on the acoustic processes in glacial bays beyond the existing literature. It demonstrates that sound energy due to SGM is concentrated at near-horizontal arrival angles at the array. These provide strong evidence that the emitted acoustic energy is highest from ice melting at shallow depths. These results demonstrate that passive acoustic monitoring is a promising tool to understand SGM, a task that is currently being done using techniques such as oceanographic flux-gate methods, buoyant plume theory, or direct active sonar measurements (Straneo and Cenedese, 2015; Sutherland *et al.*, 2019). Passive monitoring could provide additional insights that are complementary to these methods.

Previous studies have shown that passive acoustic monitoring can be used to quantify calving fluxes (Glowacki and Deane, 2020). A vertical array can provide more valuable information for the characterization of calving fluxes at glaciers such as the depth of submarine calving events along with their trajectory of movement. An array can also capture the time-varying directionalities due to moving pieces of ice in the bay, which approach close enough so that their sound is distinguishable. This allows us to acoustically track these bodies of ice, extending insights obtained from earlier related works on this (Glowacki *et al.*, 2018). This could

potentially be used to aid tracking systems to track ice pieces with good spatial and temporal coverage. It also gives us an opportunity to learn more about the glacier by using growlers or bergy-bits as proxies for the glacier because they originate from calving off it. Since it may be hard to get close enough to the glacier to perform acoustic monitoring with good resolution, studying these ice pieces opportunistically with better vertical resolution is an easier alternative.

Analysis of the vertical coherence reveals that sensors placed within the near-surface GMW duct may exhibit coherence with each other but are incoherent with sensors below the duct. An exception to this is observed during loud calving events at low frequencies where the duct has a vertical span on the same order as the acoustic wavelength and cannot trap sound. This observation also matches a similar study done earlier (Glowacki *et al.*, 2016). The GMW duct span in other regions, such as Greenland and Antarctica, is larger and can trap lower-frequency sound (Cape *et al.*, 2019; Jacobs *et al.*, 2011; Jenkins and Jacobs, 2008; Straneo *et al.*, 2011). The takeaway here is that, when using acoustic equipment in the glacial bay, careful planning must be undertaken to account for the thermohaline properties while having the source's spectral properties in mind. If an array with a larger vertical aperture than the height of the GMW duct is to be used, the sensors should be placed below the duct in order to avoid distortions from it. This is especially true if one wishes to operate at higher frequencies such as in the case of monitoring SGM.

If one wishes to deploy acoustic equipment in these regions for applications such as localization, communication, or navigation, the acoustic interference from SGM needs to be accounted for. This may be done, for example, by ensuring acoustic equipment is separated with sufficient vertical spacing so that it can reject interference from the SGM in the horizontal band based on direction. During beamforming, nulls can be steered toward the near-horizontal band to reject the SGM sound. During channel estimation for underwater communication, this information can be translated into suitable constraints. The time-varying interferences from ice pieces may pose a tougher problem due to their unpredictability. These would occur more frequently in seasons with higher calving activity. The results in this study can help guide deployment strategy to mitigate the effect of these time-varying acoustic interferences, too. For example, our observations show that most of the energy from these sources arrives at large positive elevation angles and are concentrated within a band. Hence, one plausible strategy could be to place the acoustic transmitters below the plane of the receivers during deployments so that we can distinguish the transmitters based on angular location.

The Bellhop-modeled AOAs of the rays from the glacier termini and ice pieces match the observed directionality patterns reasonably. The patterns are also consistent with environmental information. The acoustic receiver was able to distinguish rays which had undergone a significant number of bottom and surface interactions. This indicates that despite the lack of complete information on bathymetry and SSP, propagation modeling can be used as a tool to better understand the physical processes occurring in the bay. This opens up the attractive possibility of using the acoustic data to further probe the environment and gather information about it via inversion.

Seen in a larger context, this study does not paint a complete picture of the acoustic field at all types of glaciers or those in Hornsund during other times of the year. For example, closer to winter and going into spring, the bays would be frozen and the sea ice would significantly alter the propagation in the channel. Ice melting, cracking, and ice–ice interactions during this period may make contributions to the sound field that are not covered in this study. Glaciers in other regions, such as Greenland or Antarctica, may have additional acoustic features due to differences in environmental conditions. Nevertheless, this study gives valuable insights about a cross section of glacier types. These can be extrapolated to other comparable glaciers based on similarities in environmental conditions.

ACKNOWLEDGMENTS

This work was possible due to the support of grants from the National Research Foundation, Prime Minister's Office, Singapore under its Marine Science Research and Development Program MSRDP P-42, U.S. Office of Naval resources Grant No. ONR-N00014-17-1-2633, National Science Foundation Grant No. OPP-1748265, the Institute of Geophysics, Polish Academy of Sciences Grant No. 2a/IGF PAN/2017, and Statutory Activities No. 3841/E-41/S/2019 of the Ministry of Science and Higher Education of Poland. We also thank the staff at the Polish Polar research station, Hornsund, for all the support they have provided and for maintaining the oceanographical monitoring with conductivity-temperature-depth profiles.

[1]An ice melange is an agglomeration of sea ice and iceberg clasts, formed when ocean currents or surface winds fail to evacuate icebergs from a fjord (Burton *et al.*, 2018).

[2]The maximum and minimum AOA predictions are plotted only for the direct and surface-reflected arrivals because the band of variation is large for higher-order rays.

[3]The directionality plot without overlaid Bellhop model predictions is available in the supplementary material for comparison. See supplementary material at https://www.scitation.org/doi/suppl/10.1121/10.0002868 for full high-resolution versions of Figs. 9 and 10 without overlaid Bellhop predictions.

Arimitsu, M. L., Piatt, J. F., and Mueter, F. (**2016**). "Influence of glacier runoff on ecosystem structure in Gulf of Alaska fjords," Mar. Ecol.: Prog. Ser. **560**(November), 19–40.

Benn, D. I., Warren, C. R., and Mottram, R. H. (**2007**). "Calving processes and the dynamics of calving glaciers," Earth-Sci. Rev. **82**(3-4), 143–179.

Błaszczyk, M., Ignatiuk, D., Uszczyk, A., Cielecka-Nowak, K., Grabiec, M., Jania, J. A., Moskalik, M., and Walczowski, W. (**2019**). "Freshwater input to the Arctic fjord Hornsund (Svalbard)," Polar Res. **38**(April), p. 3506.

Błaszczyk, M., Jania, J. A., and Kolondra, L. (**2013**). "Fluctuations of tidewater glaciers in Hornsund Fjord (Southern Svalbard) since the beginning of the 20th century," Pol. Polar Res. **34**(4), 327–352.

Buckingham, M. J. (**1981**). "Spatial coherence of wind-generated noise in a shallow ocean channel," J. Acoust. Soc. Am. **70**(5), 1412–1420.

Buckingham, M. J. (**1997**). "Source depth and the spatial coherence of ambient noise in the ocean," J. Acoust. Soc. Am. **102**(5), 2637–2644.
Burton, J. C., Amundson, J. M., Cassotto, R., Kuo, C. C., and Dennin, M. (**2018**). "Quantifying flow and stress in ice mélange, the world's largest granular material," Proc. Natl. Acad. Sci. U.S.A. **115**(20), 5105–5110.
Cape, M. R., Vernet, M., Pettit, E. C., Wellner, J., Truffer, M., Akie, G., Domack, E., Leventer, A., Smith, C. R., and Huber, B. A. (**2019**). "Circumpolar deep water impacts glacial meltwater export and coastal biogeochemical cycling along the west Antarctic Peninsula," Front. Mar. Sci. **6**(MAR), 1–23.
Carper, S. A. (**2017**). "Low frequency active sonar performance in the Arctic Beaufort Lens," Ph.D. thesis, Massachusetts Institute of Technology, Cambridge, MA.
Collins, M. D., Turgut, A., Menis, R., and Schindall, J. A. (**2019**). "Acoustic recordings and modeling under seasonally varying sea ice," Sci. Rep. **9**(1), 1–11.
Cox, H. (**1973**). "Spatial correlation in arbitrary noise fields with application to ambient sea noise," J. Acoust. Soc. Am. **54**(5), 1289–1301.
Cron, B. F., and Sherman, C. H. (**1962**). "Spatial-correlation functions for various noise models," J. Acoust. Soc. Am. **34**(11), 1732–1736.
Deane, G. B., Buckingham, M. J., and Tindle, C. T. (**1997**). "Vertical coherence of ambient noise in shallow water overlying a fluid seabed," J. Acoust. Soc. Am. **102**(6), 3413–3424.
Deane, G. B., and Glowacki, O. (**2018**). "The vertical directionality of melt noise from a glacier terminus," J. Acoust. Soc. Am. **143**(3), 1833–1833.
Deane, G. B., Glowacki, O., Dale Stokes, M., and Pettit, E. (**2019**). "The underwater sounds of glaciers," Acoust. Today **15**(4), 12–19.
Deane, G. B., Glowacki, O., Tegowski, J., Moskalik, M., and Blondel, P. (**2014**). "Directionality of the ambient noise field in an Arctic, glacial bay," J. Acoust. Soc. Am. **136**(5), EL350–EL356.
Dziak, R. P., Bohnenstiehl, D. W. R., Stafford, K. M., Matsumoto, H., Park, M., Lee, W. S., Fowler, M. J., Lau, T. K., Haxel, J. H., and Mellinger, D. K. (**2015**). "Sources and levels of ambient ocean sound near the Antarctic Peninsula," PLoS One **10**(4), 1–23.
Earth Resources Observation and Science (EROS) Center (**2020**). "USGS EROS Archive—Sentinel-2," available at www.usgs.gov/centers/eros/science/usgs-eros-archive-sentinel-2?qt-science_center_objects=0#qt-science_center_objects (Last viewed December 2020).
Freitag, L., Ball, K., Partan, J., Koski, P., and Singh, S. (**2016**). "Long range acoustic communications and navigation in the Arctic," in *OCEANS 2015—MTS/IEEE Washington*.
Freitag, L., Singh, S., Ball, K., Johnson, T., Giaya, D., Muenchow, A., and Washam, P. (**2019**). "Experimental results in acoustic communications under shore-fast Greenland ice," in *OCEANS 2019—Marseille*, IEEE, pp. 1–6.
Gautier, D. L., Bird, K. J., Charpentier, R. R., Grantz, A., Houseknecht, D. W., Klett, T. R., Moore, T. E., Pitman, J. K., Schenk, C. J., Schuenemeyer, J. H., Sorensen, K., Tennyson, M. E., Valin, Z. C., and Wandrey, C. J. (**2009**). "Assessment of undiscovered oil and gas in the Arctic," Science **324**(5931), 1175–1179.
Glasser, N. F. (**2011**). "Polythermal glaciers," in *Encyclopedia of Snow, Ice and Glaciers. Encyclopedia of Earth Sciences Series*, edited by V. Singh, P. Singh, and U. Haritashya (Springer, Dordrecht), pp. 865–867.
Glowacki, O. (**2020**). "Underwater noise from glacier calving: Field observations and pool experiment," J. Acoust. Soc. Am. **148**(1), EL1–EL7.
Glowacki, O., and Deane, G. B. (**2020**). "Quantifying iceberg calving fluxes with underwater noise," Cryosphere **14**(3), 1025–1042.
Glowacki, O., Deane, G. B., and Moskalik, M. (**2018**). "The intensity, directionality, and statistics of underwater noise from melting icebergs," Geophys. Res. Lett. **45**(9), 4105–4113, https://doi.org/10.1029/2018GL077632.
Głowacki, O., Deane, G. B., Moskalik, M., Tęgowski, J., and Blondel, P. (**2015**). "Two-element acoustic array gives insight into ice-ocean interactions in Hornsund Fjord, Spitsbergen," Pol. Polar Res. **36**(4), 355–367.
Glowacki, O., Moskalik, M., and Deane, G. B. (**2016**). "The impact of glacier meltwater on the underwater noise field in a glacial bay," J. Geophys. Res.: Oceans **121**(12), 8455–8470.
Hamilton, E. L. (**1976**). "Sound attenuation as a function of depth in the sea floor," J. Acoust. Soc. Am. **59**(3), 528–535.
Harrison, C. H. (**1996**). "Formulas for ambient noise level and coherence," J. Acoust. Soc. Am. **99**(4), 2055–2066.
Hines, P. C., Nams, D., Deveau, T., Kessel, R., Hamilton, J., Whitt, C., and Barclay, D. R. (**2018**). "Estimating channel capacity and sonar performance in the changing arctic," J. Acoust. Soc. Am. **144**(3), 1818–1819.
Jacobs, S. S., Jenkins, A., Giulivi, C. F., and Dutrieux, P. (**2011**). "Stronger ocean circulation and increased melting under Pine Island Glacier ice shelf," Nat. Geosci. **4**(8), 519–523.
Jenkins, A., and Jacobs, S. (**2008**). "Circulation and melting beneath George VI ice shelf, Antartica," J. Geophys. Res.: Oceans **113**(4), 1–18, https://doi.org/10.1029/2007JC004449.
Kinda, G. B., Simard, Y., Gervaise, C., Mars, J. I., and Fortier, L. (**2013**). "Under-ice ambient noise in Eastern Beaufort Sea, Canadian Arctic, and its relation to environmental forcing," J. Acoust. Soc. Am. **134**(1), 77–87.
Kinda, G. B., Simard, Y., Gervaise, C., Mars, J. I., and Fortier, L. (**2015**). "Arctic underwater noise transients from sea ice deformation: Characteristics, annual time series, and forcing in Beaufort Sea," J. Acoust. Soc. Am. **138**(4), 2034–2045.
Kuperman, W. A. (**1980**). "Spatial correlation of surface generated noise in a stratified ocean," J. Acoust. Soc. Am. **67**(6), 1988–1996.
Lewis, J. K., and Denner, W. W. (**1988**). "Higher frequency ambient noise in the Arctic Ocean," J. Acoust. Soc. Am. **84**(4), 1444–1455.
Macpherson, J. D. (**1962**). "Some under-ice acoustic ambient noise measurements," J. Acoust. Soc. Am. **34**(8), 1149–1150.
Michalopoulou, Z. H., and Porter, M. B. (**1996**). "Matched-field processing for broad-band source localization," IEEE J. Ocean Eng. **21**(4), 384–391.
Miller, A. W., and Ruiz, G. M. (**2014**). "Arctic shipping and marine invaders," Nat. Clim. Change **4**(6), 413–416.
Milne, A. R., and Ganton, J. H. (**1964**). "Ambient noise under Arctic-Sea ice," J. Acoust. Soc. Am. **36**(5), 855–863.
Moffat, C., and Meredith, M. (**2018**). "Shelf-ocean exchange and hydrography west of the Antarctic Peninsula: A review," Philos. Trans. R. Soc., A **376**(2122), 20170164.
Moskalik, M., Grabowiecki, P., Tęgowski, J., and Żulichowska, M. (**2013**). "Bathymetry and geographical regionalization of Brepollen (Hornsund, Spitsbergen) based on bathymetric profiles interpolations," Pol. Polar Res. **34**(1), 1–22.
Muckenhuber, S., Nilsen, F., Korosov, A., and Sandven, S. (**2016**). "Sea ice cover in Isfjorden and Hornsund, Svalbard (2000–2014) from remote sensing data," Cryosphere **10**(1), 149–158.
National Snow and Ice Data Center "Bergy-bit—Cryosphere Glossary," available at https://nsidc.org/cryosphere/glossary/term/bergy-bit (Last viewed December 2020).
National Snow and Ice Data Center "Growler—Cryosphere Glossary," available at https://nsidc.org/cryosphere/glossary/term/growler (Last viewed December 2020).
Oppenheimer, M., Glavovic, B., Hinkel, J., van de Wal, R., Magnan, A., Abd-Elgawad, A., Cai, R., Cifuentes-Jara, M., DeConto, R., Ghosh, T., Hay, J., Isla, F., Marzeion, B., Meyssignac, B., and Sebesvari, Z. (**2019**). "Sea level rise and implications for low-lying islands, coasts and communities," in *IPCC Special Report on the Ocean and Cryosphere in a Changing Climate*, edited by H.-O. Portner, D. Roberts, V. Masson-Delmotte, P. Zhai, M. Tignor, E. Poloczanska, K. Mintenbeck, A. Alegria, M. Nicolai, A. Okem, J. Petzold, B. Rama, and N. M. Weyer (to be published).
Overland, J. E., Hanna, E., Hanssen-Bauer, I., Kim, S. J., Walsh, J. E., Wang, M., Bhatt, U. S., and Thoman, R. L. (**2017**). "Surface air temperature [in Arctic Report Card 2017]," Technical Report, available at www.arctic.noaa.gov/Report-Card (Last viewed December 2020).
Pettit, E. (**2012**). "Passive underwater acoustic evolution of a calving event," Ann. Glaciol. **53**(60), 113–122.
Pettit, E., Lee, K. M., Brann, J. P., Nystuen, J. A., Wilson, P. S., and Neel, S. O. (**2015**). "Unusually loud ambient noise in tidewater glacier fjords: A signal of ice melt," Geophys. Res. Lett. **42**(7), 2309–2316, https://doi.org/10.1002/2014GL062950.
Pettit, E., Nystuen, J., and O'Neel, S. (**2012**). "Listening to glaciers: Passive hydroacoustics near marine-terminating glaciers," Oceanography **25**(3), 104–105.
Porter, M. B. (**2011**). "The BELLHOP Manual and User's Guide: Preliminary draft," in *Tech. Rep.* (Heat, Light and Sound Research, Inc., La Jolla, CA, 2011).
Porter, M. B., and Bucker, H. P. (**1987**). "Gaussian beam tracing for computing ocean acoustic fields," J. Acoust. Soc. Am. **82**(4), 1349–1359.
Poulsen, A. J., and Schmidt, H. (**2016**). "Acoustic noise properties in the rapidly changing Arctic Ocean," Proc. Mtgs. Acoust. **28**(1), 070005.

Pritchard, R. S. (**1990**). "Sea ice noise-generating processes," J. Acoust. Soc. Am. **88**(6), 2830–2842.
Sagen, H., Johannessen, O. M., and Sandven, S. (**1990**). "The influence of sea ice on ocean ambient sound," in *Ice Technology for Polar Operations*, edited by P. W. T. K. S. Murthy, J. G. Paren, and W. M. Sackinger (Computational Mechanics Publications, Cambridge, England).
Sanjana, M. C., Latha, G., Thirunavukkarasu, A., and Venkatesan, R. (**2018**). "Ambient noise field and propagation in an Arctic fjord Kongsfjorden, Svalbard," Polar Sci. **17**(July), 40–49.
Scholander, P. F., and Nutt, D. C. (**1960**). "Bubble pressure in Greenland icebergs," J. Glaciol. **3**(28), 671–678.
Schulz, M., Berger, W. H., and Jansen, E. (**2008**). "Listening to glaciers," Nat. Geosci. **1**(7), 408–408.
Staszek, M. W., and Moskalik, M. J. (**2015**). "Contemporary sedimentation in the forefield of Hornbreen, Hornsund," Open Geosci. **7**(1), 000010151520150042.
Straneo, F., and Cenedese, C. (**2015**). "The dynamics of Greenland's glacial fjords and their role in climate," Ann. Rev. Mar. Sci. **7**(1), 89–112.
Straneo, F., Curry, R. G., Sutherland, D. A., Hamilton, G. S., Cenedese, C., Våge, K., and Stearns, L. A. (**2011**). "Impact of fjord dynamics and glacial runoff on the circulation near Helheim Glacier," Nat. Geosci. **4**(5), 322–327.
Straneo, F., Heimbach, P., Sergienko, O., Hamilton, G., Catania, G., Griffies, S., Hallberg, R., Jenkins, A., Joughin, I., Motyka, R., Pfeffer, W. T., Price, S. F., Rignot, E., Scambos, T., Truffer, M., and Vieli, A. (**2013**). "Challenges to understanding the dynamic response of Greenland's marine terminating glaciers to oceanic and atmospheric forcing," Bull. Am. Meteorol. Soc. **94**(8), 1131–1144.
Straneo, F., Sutherland, D. A., Holland, D., Gladish, C., Hamilton, G. S., Johnson, H. L., Rignot, E., Xu, Y., and Koppes, M. (**2012**). "Characteristics of ocean waters reaching Greenland's glaciers," Ann. Glaciol. **53**(60), 202–210.
Sutherland, D. A., Jackson, R. H., Kienholz, C., Amundson, J. M., Dryer, W. P., Duncan, D., Eidam, E. F., Motyka, R. J., and Nash, J. D. (**2019**). "Direct observations of submarine melt and subsurface geometry at a tidewater glacier," Science **365**(6451), 369–374.
Tegowski, J., Deane, G. B., Lisimenka, A., and Blondel, P. (**2011**). "Underwater ambient noise of glaciers on Svalbard as indicator of dynamic processes in the Arctic," in *4th International Conference and Exhibition on "Underwater Acoustic Measurements: Technologies & Results,"* Kos, Greece, pp. 1149–1154.
Tegowski, J., Deane, G. B., Lisimenka, A., and Blondel, P. (**2012**). "Spectral and statistical analyses of ambient noise," Proc. Mtgs. Acoust. **17**, 070079.
Urick, R. J. (**1971**). "The noise of melting icebergs," J. Acoust. Soc. Am. **50**(1B), 337–341.
Wawrzyniak, T., and Osuch, M. (**2020**). "A 40-year high Arctic climatological dataset of the Polish Polar Station Hornsund (SW Spitsbergen, Svalbard)," Earth Syst. Sci. Data **12**(2), 805–815.
Zakarauskas, P., and Thorleifson, J. M. (**1991**). "Directionality of ice cracking events," J. Acoust. Soc. Am. **89**(2), 722–734.
Zhang, Z. Y. (**2014**). "Directionality and coherence of underwater noise and their impact on sonar array performance," in *Internoise 2014—43rd International Congress on Noise Control Engineering: Improving the World Through Noise Control*, Fremantle, Australia, pp. 1–10.